An Investigation on Quench Cracking Behavior of Superalloy Udimet 720LI Using a Fracture Mechanics Approach

J. Mao, V.L. Keefer, K.-M. Chang, and D. Furrer

(Submitted 1 September 1999; in revised form 9 November 1999)

Quench cracking can be a serious problem in the heat treatment of high strength superalloys. A new fracture mechanics approach, quench cracking toughness (K_Q), was introduced to evaluate the on-cooling quench cracking resistance of superalloy Udimet 720LI. A fully automatic computer controlled data acquisition and processing system was set up to track the on-cooling quenching process and to simulate the quench cracking. The influences of grain size, cooling rate, solution temperature, and alloy processing routes on quench cracking resistance were investigated. Research results indicate that quench cracking revealed a typical brittle and intergranular failure at high temperatures, which causes a lower quench cracking toughness in comparison to fracture toughness at room temperature. Fine grain structures show the higher quench cracking resistance and lower failure temperatures than intermediate grain structures at the same cooling rates. Moreover, higher cooling rate results in lower cracking toughness under the same grain size structures. In comparison of processing routes, powder metallurgy (PM) alloys show higher cracking resistance than cast and wrought (CW) alloys for fine grain structures at the same cooling rates. However, for intermediate grain structure, there is no obvious difference of K_Q between the two processing routes in this study.

Keywords cast and wrought, cooling rate, fracture mechanics, grain size, heat treatment, powder metallurgy, quench cracking, superalloy, Udimet 720

1. Introduction

Heat treatment is one of the most important factors affecting superalloy performance. The higher the cooling rate from solution temperature, the higher the supersaturation of precipitation hardening elements, which results in an increase in the number of fine precipitates that are distributed homogeneously throughout the matrix and therefore in higher strength of the alloy. Many research efforts have been devoted to attaining more benefit from heat treatment, especially by achieving maximum cooling rate. However, superalloy is so sensitive to its cooling rate that aggressive cooling usually causes problems such as severe distortion and even quench cracking due to excessive thermal stress.[1,2] Furthermore, the development of a new generation of damage-tolerant superalloys requires superalloys to be subjected to a supersolvus temperature solution cycle in order to produce coarse grain structure, which engenders an enhanced fatigue crack propagation resistane.[3,4] In this case, quench distortion and cracking become a more serious issue. Therefore, for large components, the selection of quenching procedure has become an art of balancing between achieving desired properties and avoiding quench cracking.[5]

J. Mao and **K.-M. Chang,** Department of Mechanical & Aerospace Engineering, West Virginia University, Morgantown, WV 26505; **V.L. Keefer,** Rt.1, Box1, Leon, WV 26505; and **D. Furrer,** Ladish Co., Inc., Cudahy, WI 53110-8902.

When a component cools down from an elevated temperature (solution temperature), thermal stress develops because of the temperature difference between the center and the surface. It is generally believed that if this thermal stress reaches up to a certain value, and exceeds the ultimate strength (or on-cooling ultimate strength[6]) of the material, quench cracking will occur. This strength criterion of cracking is currently used in heat treatment simulation. But it is difficult to explain why a very thin layer of preventive nickel plating on the surface of a component can offer a solution to preventing quench cracking.[7,8] Nowadays most quenching modeling focuses on the prediction of cooling rates and mechanical properties in worked parts and the calculation of residual stresses and distortion due to aggressive cooling rate during quenching.[9,10] The problem of how to predict the exact occurrence of quench cracking and to evaluate the quench cracking resistance of superalloys has not yet been solved.

In addition, since randomized surface defects, such as inclusions, machining scratches, and other surface discontinuities, in superalloy components are inevitable, it is not surprising that the strength analysis method cannot accurately predict the occurrence of quench cracking. A more reasonable approach is to use the fracture mechanics method to evaluate quench cracking resistance. The quench cracking toughness approach has been adapted and has brought out some significant results in the investigation of quench cracking resistance of the powder metallurgy (PM) superalloy Rene'95.[11]

In this study, we focus on superalloy Udimet 720LI, which can be processed by either cast and wrought (CW) or PM routes. This alloy has received great interest in the turbine engine community.[12–14] The fracture mechanics approach, quench cracking toughness, was used to evaluate its quench resistance. Several influencing factors, including grain size, processing routes, cooling rate, and solution temperature, were investigated.

Table 1 Udimet 720LI composition, wt.%

	C	W	Mo	Zr	B	Fe	Co	Cr	Al	Ti	Ni
PM U720Li	0.025	1.30	3.02	0.035	0.017	0.06	14.75	16.35	2.46	4.99	Bal
CW U720Li	0.013	1.18	2.85	0.030	0.014	0.14	14.45	16.14	2.48	5.15	Bal
Udimet 720(a)	0.035	1.25	3.0	0.03	0.033	. . .	14.7	18.0	2.5	5.0	Bal

(a) From Ref 13

Table 2 The processing routes and quench test parameters of PM and CW Udimet 720LI superalloys

	Processing routes	PMFG	PMIG	PMCG	CWFG	CWIG
As-received specimen condition	Forging method	Isothermal			Isothermal + hot die	
	Solution temperature	No	Supersolvus		Subsolvus	Nearsolvus
	Aging	No	Double aging			
Quench test parameter	Solution temperature	Subsolvus		Supersolvus		Subsolvus
	Cooling rates	150 °C/min, 600 °C/min				

2. Materials and Experimental Procedure

2.1 Materials

The specimens used in this study were prepared and supplied by Ladish Co., Inc. (Cudahy, WI). Table 1 shows the measured chemical compositions (wt.%) of the materials investigated. These alloys are designated as U720LI, which contains lower C, B, and Cr contents compared to the original version of U720.

The processing routes of materials are summarized in Table 2. In the specimen designation, (PM and CW stand for materials processed by powder metallurgy and cast and wrought routes, respectively). All the PM materials were processed by the standard isothermal forge operation. The CW materials were processed by isothermal and hot-die forging operation. The samples were also identified as FG, IG, and CG to denote fine grain, intermediate grain, and coarse grain sīze microstructures, respectively. Of all the materials as-received, only PMFG is in as-forged fine grain state. The remaining samples had already undergone solution treatment and double aging processes after forging. PMIG and PMCG refer to PM materials with grain structures obtained from supersolvus temperature solutioning. Subsolvus and nearsolvus solution treatments were applied to the CW materials to produce fine grain structure (CWFG) and intermediate grain structure (CWIG), respectively. In our quenching tests, all specimens except PMCG were quenched from subsolvus temperature (1107 °C). PMCG specimens were quenched from supersolvus temperature (1168 °C).

2.2 Precrack

Dog-bone-shaped sheet specimen with single edge notch was used in this study. Fig. 1 shows the schematic drawing of the specimen.

Precracking was performed at room temperature on an MTS 810 hydraulic close-loop machine. A constant stress concentration factor ($\Delta K \approx 27$ MPa$\sqrt{m}$) was used in the precracking. The precrack length was controlled automatically based on potential drop and also monitored by a microscope. Final precrack length (a) was measured on the fracture surface of the failed specimen according to the ASTM E339 standard. Most of the precrack lengths were controlled to be in the range of $0.45 < a/w < 0.55$, where a is the crack length and w is the width of the specimen.

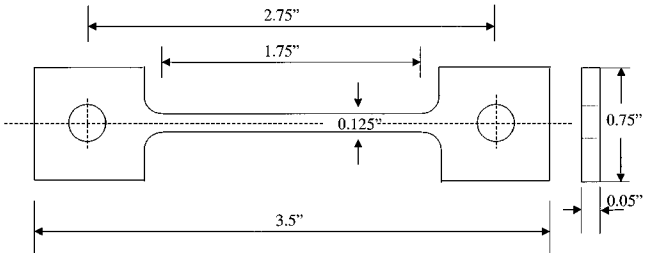

Fig. 1 Scheme of quench cracking specimen

2.3 Quench Cracking

Quench cracking tests were performed on the same MTS 810 machine mounted with a high power quartz furnace. Because of the low thermal capacity of the system, both heating and cooling rates can be controlled. Two pairs of thermal couple were spot welded directly on each side of the specimen. The location of the welding spots was just below the precracks. On-cooling temperature and induced thermal load were monitored automatically through computer data acquisition and processing system.

Specimens were held on the machine and heated up to the designated temperatures (1168 °C for PMCG specimens and 1107 °C for all the other specimens) at controlled heating rates. Load on the specimen was kept at a minimum positive value. When the temperature of a specimen was stabilized, the system was switched to displacement control (a constant fixed displacement), and the quenching at a given cooling rate (150 and 600 °C/min) was activated. With the temperature decreasing, the quenching stress (load) on the specimen induced by thermal contraction increases. The stress intensity factor K was converted from Tada's empirical equation according to on-cooling load and the precrack length:[15]

$$K = \frac{P}{B\sqrt{W}} \frac{\sqrt{2\tan\frac{\pi a}{2w}}}{\cos\frac{\pi a}{2w}} \left[0.752 + 2.02\left(\frac{a}{w}\right) + 0.37\left(1 - \sin\frac{\pi a}{2w}\right)^3 \right]$$

where

a = precrack length at the onset of quenching, measured from failed specimen;
W = the width of specimen;
B = the thickness of specimen; and
P = the load recorded during quenching.

Quench cracking is incurred when K reaches a certain value at which cracking occurs or maximum load is reached, which is defined as the quench cracking toughness, K_Q. The temperature at which K_Q is achieved is defined as the failing temperature.

2.4 Microstructure and Fracture Analysis

Fractured specimens were observed under a scanning electron microscope (SEM) to investigate the fracture modes. Metallography samples were prepared by standard laboratory procedures. Electrolytic-polish and electrolytic-etch methods were used to reveal the γ' precipitates morphology. The electrolytic-etch solution was chromium acid solution (170 mL H_3PO_4 + 16 g CrO_3 + 10 mL H_2SO_4). Chemical etching was used to study the grain structure. The chemical etchant used is 50 mL HCL + 50 mL H_2O + 1 mL H_2O_2.

Differential thermal analysis (DTA) was carried out on thermal analysis DTA1600 to identify the γ' solvus temperature of PM and CW U720LI superalloys. The device is calibrated to the precision within 1 °C of melting temperature of pure nickel. The heating and cooling rate during the DTA test was 10 °C/min.

3. Results

3.1 Microstructure of the Materials

Differential thermal analysis indicated that the γ' solvus temperatures of CW and PM alloys are about 1137 and 1126 °C, respectively. The full dissolution temperature of γ' is about 1155 °C. Therefore, in our study, except PMCG, which was quenched from the supersolvus temperature 1168 °C, all the other tests were quenched from a subsolvus temperature (1107 °C), as seen in Table 2.

As-Received Materials. The grain structure and γ' precipitate distribution of as-received PM and CW U720LI alloys are shown in Fig. 2 and 3. The structures of the materials used in the experiment are consistent with other investigations.[14–17] Grain sizes in PMFG and CWFG (ASTM 10–12) are much finer than those in PMIG and CWIG (ASTM 6–8), which is the result of an as-forged status for PMFG and a subsolvus temperature solution after forging for CWFG. Blocky γ' particles (about 3 to 5 μm in diameter) in PMFG and CWFG, known as primary γ' precipitates, serve as pinning points, preventing the grain growth in both PMFG and CWFG structures. No blocky γ' precipitates are visible in as-received PMIG, CWIG, and PMCG because of the supersolvus or near-solvus temperature solution after forging.

As-Quenched Materials. After quench test, the grain size and the morphology of blocky primary γ' in all the samples

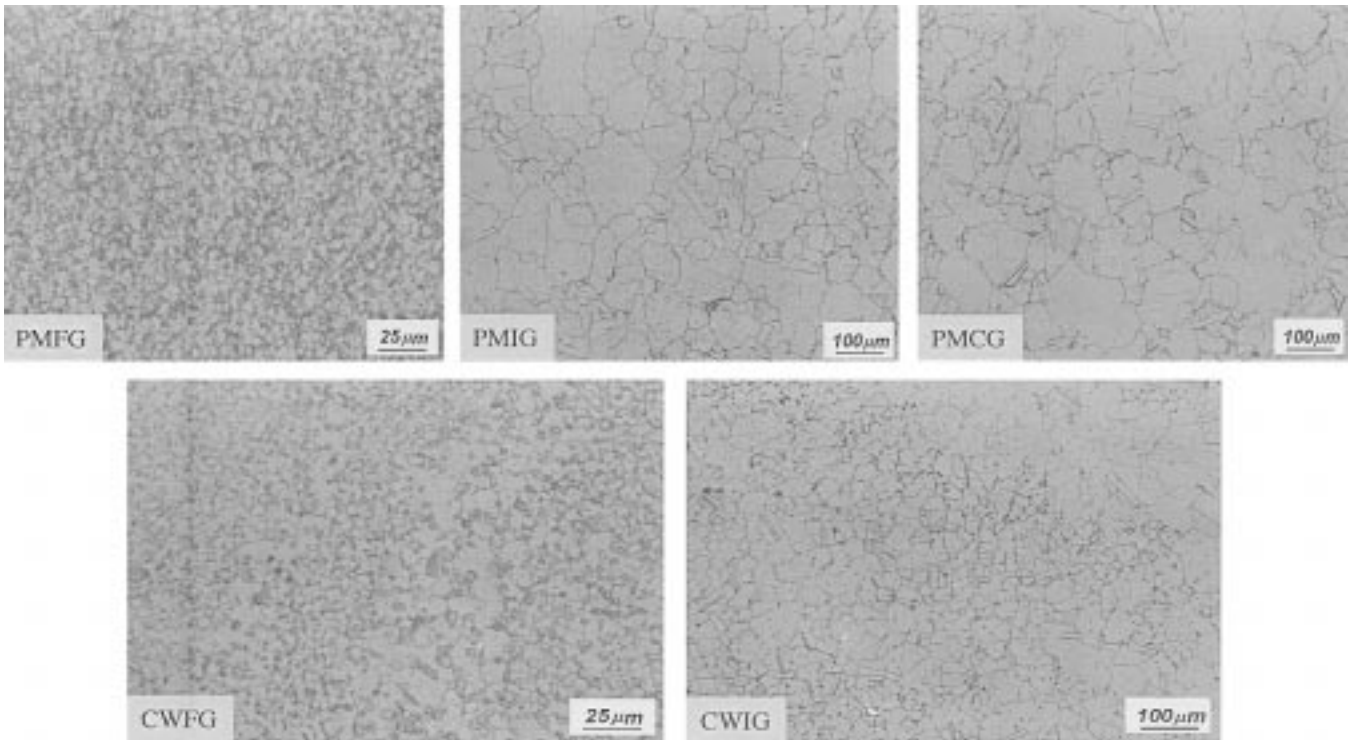

Fig. 2 Grain structure of PM and CW Udimet720LI superalloys

remained predominately the same as in the as-received structure. The reason for IG structure remaining without primary γ' is that there is not enough time for IG samples to grow blocky γ' during the 1107 °C subsolvus temperature quenching test.

In contrast to PM alloys, the grain structures in CW alloys are evidently inhomogeneous, which is believed to be associated with the chemical segregation during ingot casting.

A number of carbide precipitates are observed along grain boundaries in both PMIG and CWIG alloys.

Precrack. Table 3 compares the precrack growth rates between fine grain and intermediate grain structures in both PM and CW U720LI. The crack growth rate for a given $\Delta K \approx 27$ MPa$\sqrt{\text{m}}$ in the fine grain structure is higher than that in the intermediate grain structure. Additionally, PM alloy demonstrates a higher crack growth rate than does CW alloy when they have almost the same grain sizes. Fractography shows that the crack propagated in a transgranular cleavage mode at room temperature**.**

3.2 On-Cooling Quench Cracking Toughness

Table 4 summarizes all of the test parameters and the measured results. Figure 4 depicts the relationship between the quench cracking toughness and the failing temperature. It is obvious that grain size has a great influence on quench cracking toughness. Finer grain structure shows a higher quench cracking toughness and a lower failing temperature, while intermediate grain structure fails at a relatively high temperature with a low K_Q value measured.

The grain size effect can also be recognized further through the comparison of the on-cooling thermal loading behavior. Stress intensity factor *K* corresponding to the thermal loading can be calculated and plotted *via* specimen temperature *T*. The precrack length was measured from the fracture surface. The *K-T* curves of tested specimens are found in Figs. 5 and 6.

For intermediate grain structure samples (Fig. 5), with the temperature decrease, the stress intensity factor *K* increases very

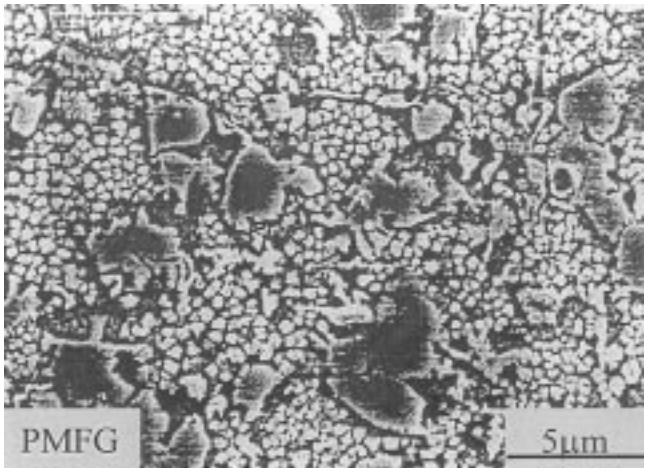

(a)

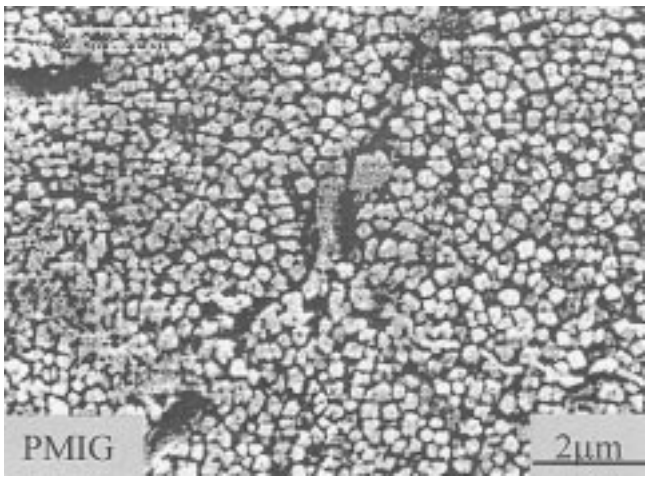

(b)

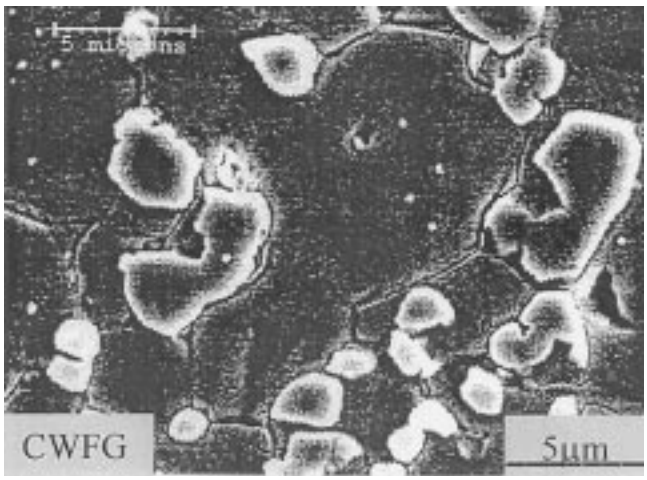

(c)

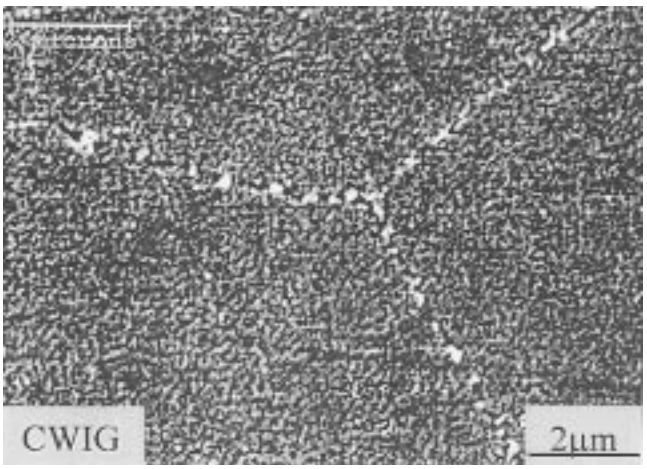

(d)

Fig. 3 γ' precipitates morphology in PM and CW Udimet720LI superalloys

Table 3 Precrack growth rates of PM and CW Udimet 720LI superalloys

	PMFG	PMIG	PMCG	CWFG	CWIG
ΔK, MPa$\sqrt{m}$	26.22	26.15	26.12	26.79	26.71
da/dN	8.17×10^{-5}	6.16×10^{-5}	5.99×10^{-5}	3.43×10^{-5}	1.55×10^{-6}
Grain size (μm)	7.3	28.3	. . .	8.6	25.5
ASTM	10.9	7.0	6(a)	10.4	7.3

(a) Data are provided by Ladish Co.

Table 4 Quench cracking resistance of PM and CW Udimet 720LI superalloys

	$T_{solution}$ (°C)	Cooling rate (°C/min)	Max load (N)	T_{fail} (°C)	K_Q (MPa $\sqrt{m}$)	a_f (mm)	a/w	Note
PMFG-1	1107	150	76.89	555	100.37	3.393	0.534	Delay
PMFG-2	1107	150	109.29	639	135.93	3.322	0.523	
PMFG-3	1107	600	77.77	617	99.51	3.364	0.530	
CWFG-1	1107	150	89.24	655	114.66	3.370	0.531	
CWFG-2	1107	600	115.51	386	73.92	2.278	0.359	
CWFG-3	1107	600	72.30	369	90.98	3.350	0.528	Delay
CWFG-4	1107	600	57.31	654	72.57	3.378	0.532	
PMIG-1	1107	150	35.91	868	48.98	3.456	0.544	
PMIG-2	1107	600	34.48	936	53.40	3.632	0.572	Preload
PMIG-3	1107	600	38.82	914	38.88	2.996	0.472	
CWIG-1	1107	150	43.95	881	40.98	2.885	0.454	
CWIG-2	1107	600	30.99	949	59.50	3.920	0.617	Preload
CWIG-3	1107	600	36.86	876	40.89	3.170	0.499	
PMCG-1	1165	150	28.62	907	38.37	3.431	0.540	Delay
PMCG-2	1165	150	29.10	954	31.60	3.133	0.493	
PMCG-3	1165	600	56.50	949	46.44	2.685	0.423	
PMCG-4	1165	600	38.88	934	41.31	3.099	0.488	

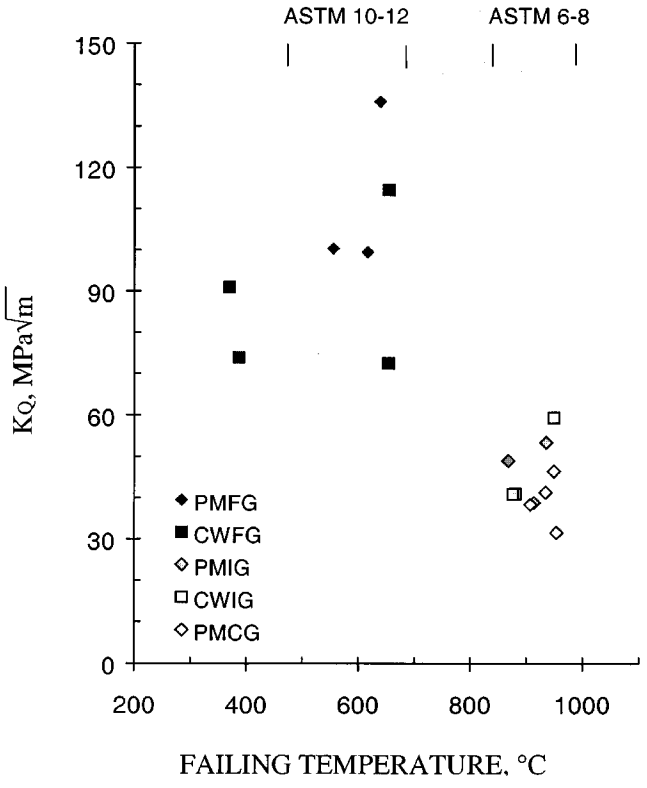

Fig. 4 Relationship between the quench cracking toughness and the failing temperature in PM and CW Udimet 720LI superalloys

quickly. Final failure comes abruptly. The K_Q is about 35 to 50 MPa$\sqrt{m}$ for both PMIG and CWIG, and the failing temperature is about 850 to 950 °C.

For fine grain structure samples, with the temperature cooling down, the K increase rate is lower than that in the intermediate grain structure at the beginning of the quenching. Furthermore, there are some zig-zags in the K-T curve just before the final catastrophic failure occurs. The K_Q for fine grain structure is higher than that in intermediate grain structure, about 60 to 120 MPa$\sqrt{m}$. Failing temperatures for both of them are in the range of 550 to 600 °C. In addition, PMFG and CWFG alloys have similar cooling and failure behavior. The K_Q of PMFG alloy (90 to 120 MPa$\sqrt{m}$) is a little higher than that of CWFG alloys (60 to 80 MPa$\sqrt{m}$). The difference in quench cracking toughness K_Q between PMFG and CWFG alloys with similar failing temperatures may be interpreted by the inhomogeneity of grain structure. To a certain degree, the size of the grain structure in front of the cracking tip influences the mode of thermal stress increase. This not only explains the differences in K_Q between PM and CW alloys, but also the variation and scatters in CW data.

In conclusion, comparing samples of different grain structures, PMFG and CWFG have much higher K_Q (maximum load) values and failed at a lower temperature than did PMIG and CWIG. It seems that the fine grain structure requires a higher thermal stress and a greater thermal difference ΔT to initiate quench cracking.

Cooling rate also has a certain influence on K_Q. In general, a higher cooling rate results in a lower quench cracking toughness and almost the same failing temperature relative to a lower cool-

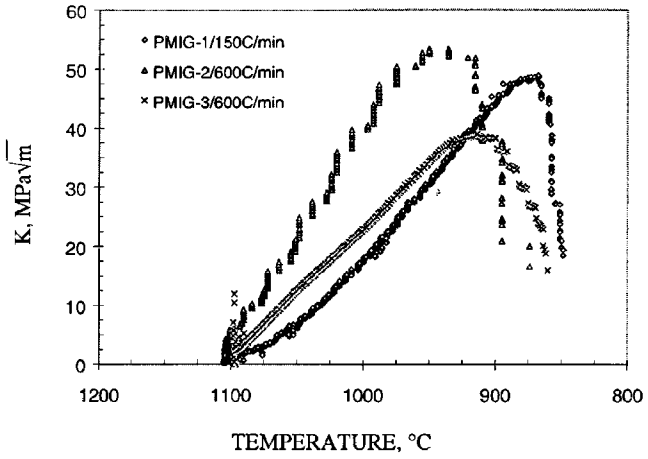

(a)

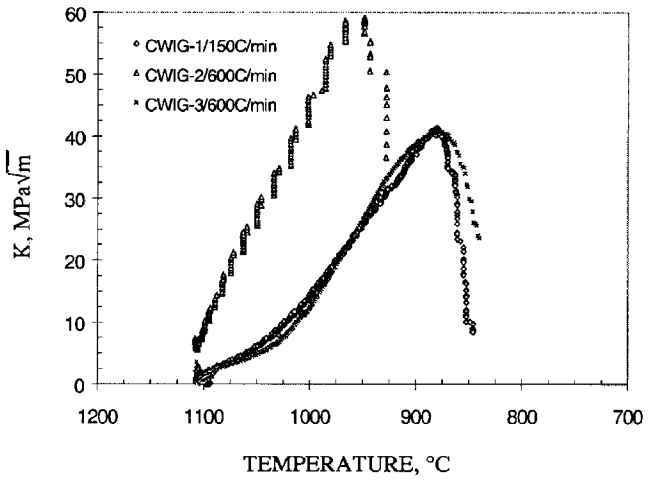

(b)

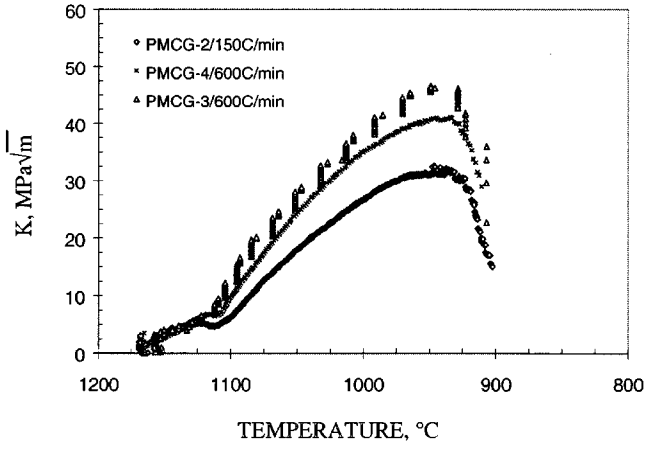

(c)

Fig. 5 *K-T* profiles of PMIG, PMCG, and CWIG Udimet 720LI superalloys

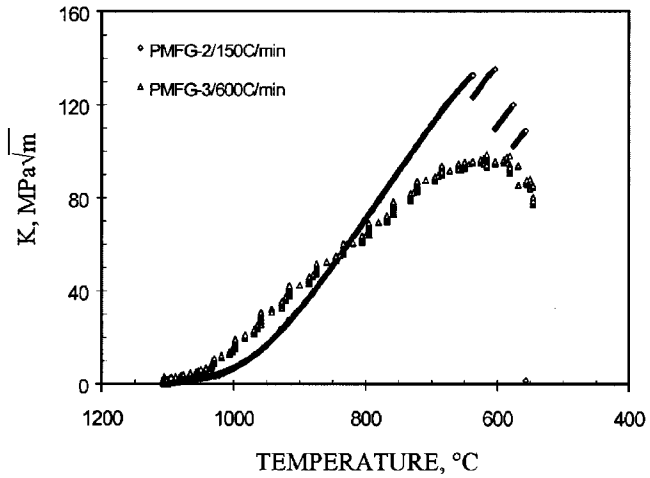

(a)

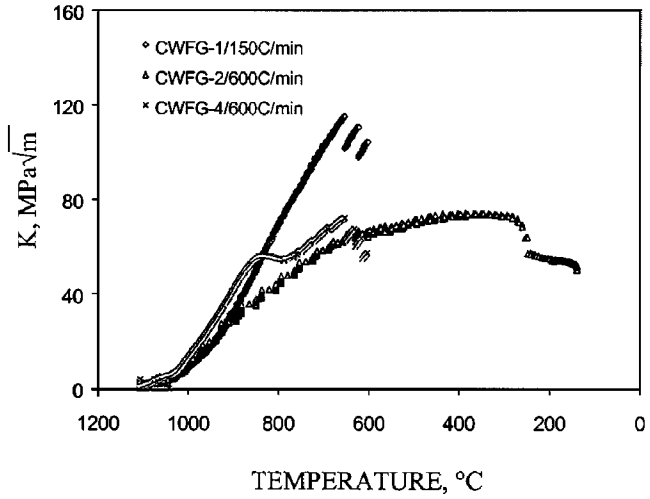

(b)

Fig. 6 *K-T* profiles of PMFG and CWFG Udimet 720LI superalloys

ing rate, with the exception of CWIG and PMCG materials, as shown in Table 4.

Solution temperature effects are demonstrated by the results of PMIG and PMCG specimens. When a specimen was quenched from supersolvus temperature, as seen in PMCG, the pickup of thermal load was slow at the beginning of the quenching. When the temperature cooled down to around the γ' solvus temperature, the thermal load started to ramp up. After that, the tendency of thermal load buildup was the same as in PMIG. However, even though there is a jump in *K-T* curve around the γ' solvus temperature, the quench cracking toughnesses in both materials are almost the same, in spite of the fact that the failing temperature is a little higher in PMCG than in PMIG (subsolvus temperature solution). It is believed that similar grain size and blocky primary γ' in both alloys are key factors determining the quench cracking resistance.

There are some special observations on some specimens. First, delay of thermal stress buildup will cause higher K_Q. At the

very beginning of quenching, if the pickup of thermal load is delayed, as seen in Fig. 7, the failing temperature will drop down below the normal failing temperature and the K_Q value will be higher than the normal value. Examples are PMFG-1 with cooling rate 150 °C/min, CWFG-3 with cooling rate 600 °C/min, and PMCG-1 with cooling rate 150 °C/min, as seen in Table 4. In these cases, the specimen had loose loading pins, because the thermal stress increment was unable to tighten the loose pins. Therefore, it is believed that these quench tests are equivalent to the tests starting at a lower temperature.

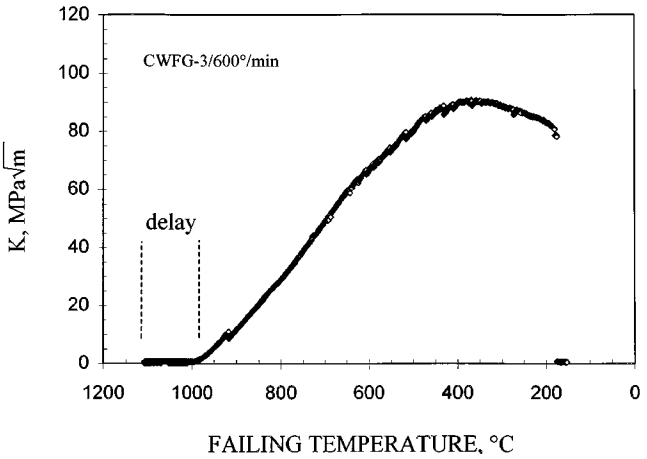

Fig. 7 The pickup of thermal stress delayed at the very beginning of the quenching

Second, a flat shape at the peak of the *K-T* curve results in a very low failing temperature. The linear increase of the stress intensity factor with the temperature drop was observed in most tests. However, specimen CWFG-2 with 600 °C/min cooling rate has a flat *K-T* curve at a peak point of the stress intensity factor and fails at very low temperatures, possibly because of the grain size variation or for some other unknown reason.

In addition, if a preload is applied on the specimen at the beginning of quenching, a higher quench toughness will be obtained. These preloading effects were demonstrated in PMIG-2 and CWIG-2 specimens. This effect could be related to the rate of loading of the precrack. Preloading effectively decreases the overall loading rate. The reason of this is still not very clear.

3.3 Fracture Modes

Fracture characteristics of ruptured specimens were examined using an SEM. Typical fracture surfaces show that two fracture modes were separated by a beach mark, as seen in Fig. 8. On the precrack side, the crack propagates in a transgranular mode for all specimens. Some fatigue striations can be seen. This is a common characteristic of fatigue fracture at room temperature. On the other side, in the quench cracking area, the fracture mode is no longer transgranular. Quench cracking propagated along grain boundaries, showing typical intergranular fracture characteristic at high temperature. No evidence of any grain boundary deformation was shown (Fig. 9), which is consistent with the result in Ref 11. This intergranular fracture phenomenon matches the cracking mode observed in disk

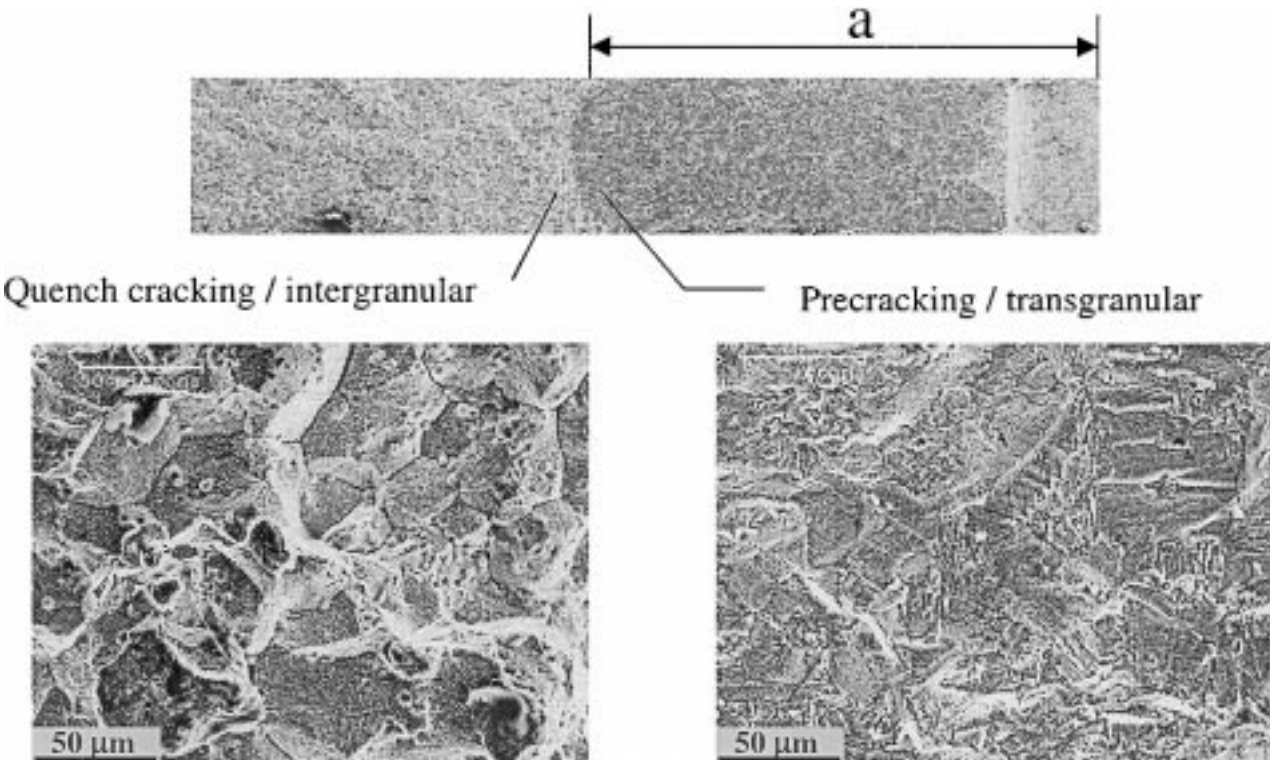

Fig. 8 Typical fracture feature in both precracking and quench cracking sides

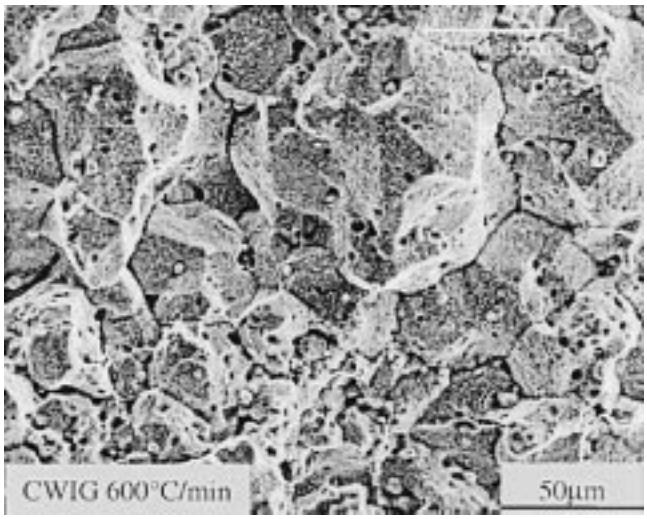

(a)

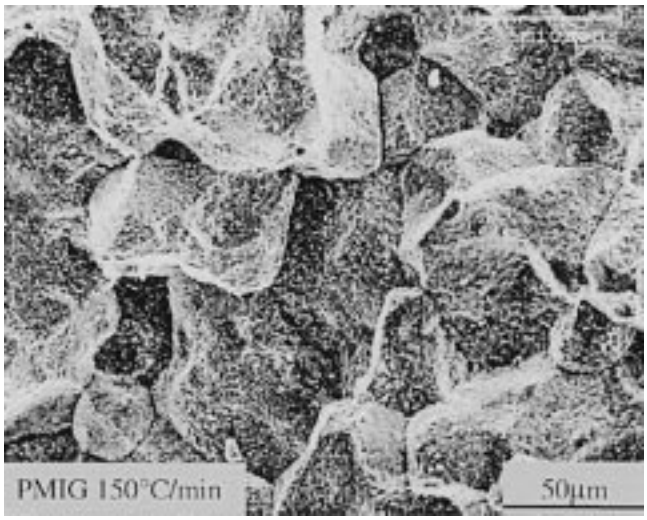

(b)

Fig. 9 Fracture morphologies in intermediate grain structures of PM and CW Udimet 720LI superalloys

quenching in practice. It is worthwhile to point out that the fracture morphology is different from that in the tensile test or stress rupture test at elevated temperature, which is usually intergranular dimple morphology for most superalloys.

Though the quench fracture modes for fine and intermediate grain structures are both intergranular, there are still some differences. For intermediate grain structure, cracking is completely brittle intergranular from the start through the end of the specimen. This kind of fracture feature is characterized by lower quench cracking resistance at higher failing temperatures.

On the other hand, in free grain structure, cracking initiated in intergranular mode. With the temperature cooling down, intergranular fracture was replaced by transgranular fracture mode, and then shear type of fracture path occurred, as shown in Fig. 10. This fracture sequence appeared in all the specimens with fine grain structures that failed at low temperatures. The fracture sequence indicates that there is a transition of fracture modes with the decrease of temperature. The transition temperature at which the fracture mode transition occurs will be an important parameter for quench process control, the investigation of which is underway.

4. Discussion

4.1. Loading Behavior

Figure 11 summarizes schematically several typical thermal loads *via* temperature curves. There are three stages of thermal load increasing during cooling. At the very beginning of quenching, both fine grain structure and intermediate grain structure undergo the strain softening process, and thus the pickup rate of thermal stress is lower. The softening in fine grain structure is more severe than in intermediate grain structure at the same cooling rate (see the inside dashed line area in Fig. 11). This characteristic is believed to be related to the deformation behavior of material at the elevated temperature. As the temperature cools down, the thermal load increases linearly, because the material strengthening process interacting with the thermal stress gradually overweighs the softening process and dominates the quench process of the alloy. After that, when the accumulation of thermal stress on the specimen with a crack or quench fracture toughness reaches a threshold, the last stage of catastrophic quench cracking occurs.

4.2 Microstructure Effect

The intermediate grain structure has a relatively lower quench cracking toughness and associated higher failing temperature, which is because intermediate and coarse grains are less compliant than fine grain and provide less obstruction of grain intersection to crack propagation and less grain boundaries to absorb cracking energy. Before the sample cools down to the transition temperature of the failure mode, rapidly increasing thermal stress reaches the critical value. The strengthening process dominates most of the quenching. In this case, once a crack is initiated, it will propagate continuously along the grain boundary. Besides, the lack of blocky γ' on grain boundaries also makes cracks easier to propagate without any obstacle. Quench cracking develops and progresses unhindered along the clean grain boundary until it arrives at the end of the fracture path.

Higher quench cracking toughness at lower failing temperature is expected in fine grain structure samples, the reason being that fine grains are more flexible and compliant to the changing of thermal stress. The softening process consumes a lot of energy at the beginning of quenching. With the temperature cooling down and the thermal stress increasing, the postponement of hardening processes makes fine grain structure materials survivable through the transition temperature. On the other hand, once a crack initiates, propagation of it along the grain boundary has to change its direction frequently because of the topographic factor of the crack path in the fine grain structure.[11] Therefore, the

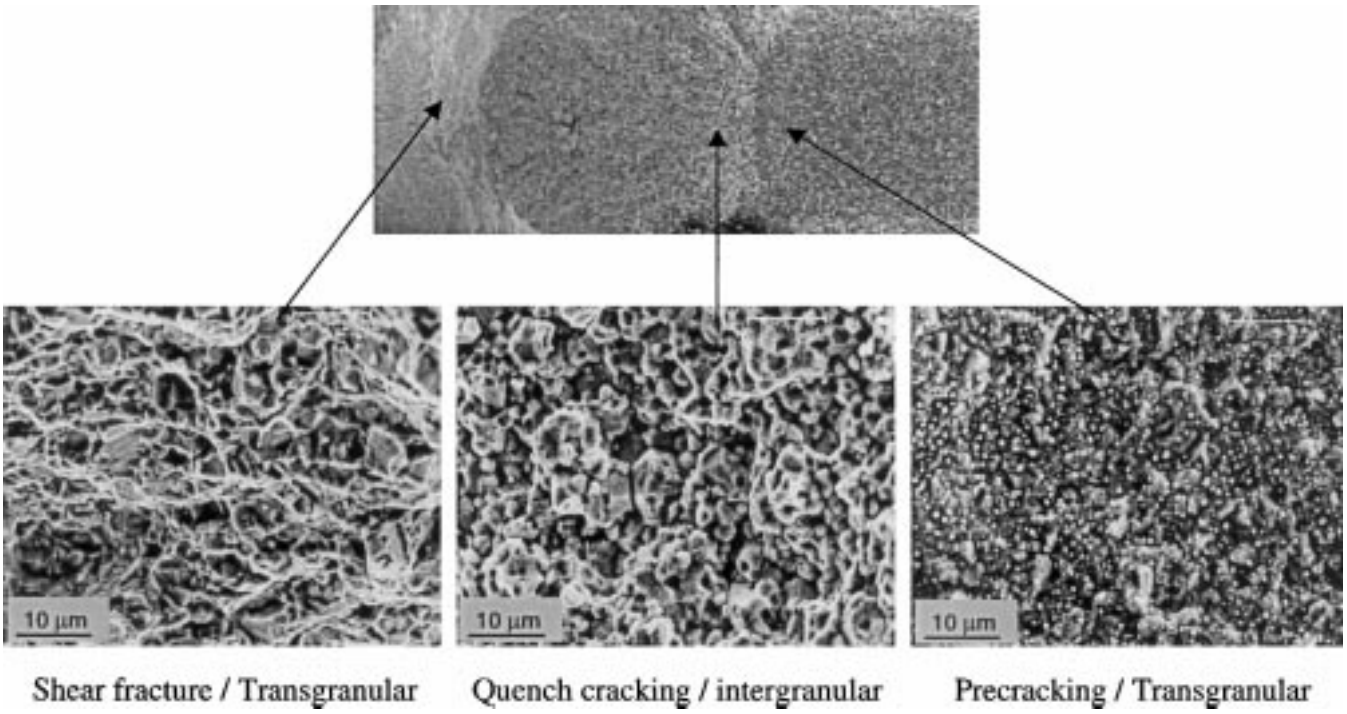

Fig. 10 Transition of fracture modes in fine grain structure

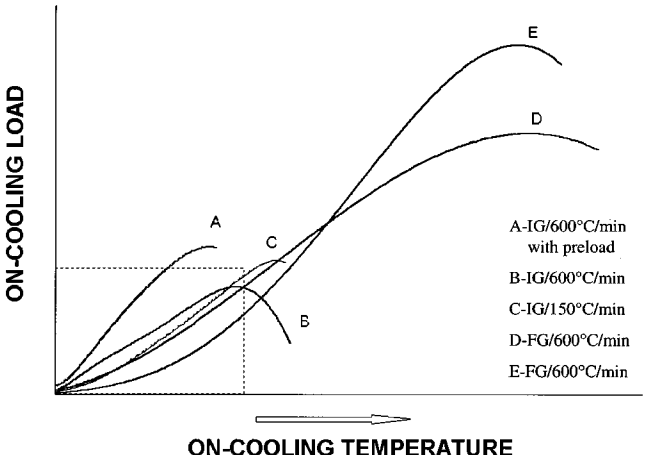

Fig. 11 Schematic on-cooling loading curves for subsolvus temperature solution. Data schematized based on the loading curves of PMFG and PMIG Udimet 720LI superalloys

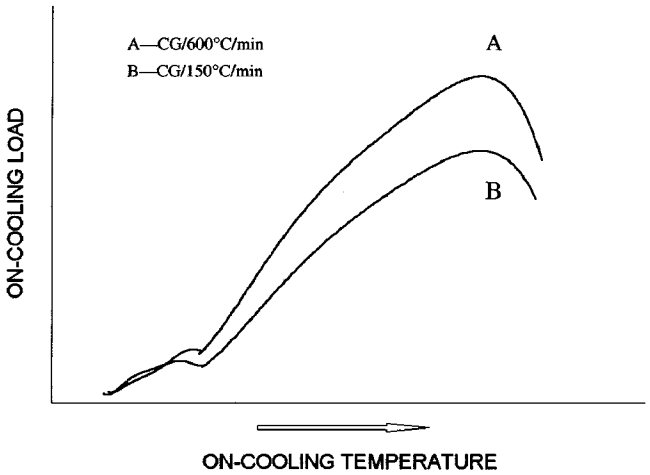

Fig. 12 Schematic on-cooling loading curves for supersolvus temperature solution in PMCG Udimet 720LI superalloy

fine grain structure can absorb much more cracking energy, taking more time to reach the critical fracture limitation before the catastrophic failure. In fact, when the temperature drops enough, intergranular cracking is actually depressed and the transition of fracture mode occurs. Blocky γ' and secondary cracks also appear to have some beneficial effects on energy release before final failure.

For PMCG materials, because of the quenching from supersolvus temperature, there is a special deformation characteristic (Fig. 12) at high temperature. There is a jumping on the *K-T* curve around the γ' solvus temperature. At the temperatures above this point, the cooling rate shows little influence on thermal stress. The reason is because all microstructure differences at or above that temperature are normalized, the alloy has very limited strength. Below the point, the kinetics of gamma-prime formation are superimposed on the cooling rate effects for thermal stress development. A similar result is reported in the on-cooling tensile test of Rene'88DT.[6] Below the jump point, thermal stress increases very quickly. Hardening overweighed the softening process, which differs from the phenomena in fine and intermediate grain structure. The hardening phenomenon is believed to be related to the preloading of spec-

Table 5 Comparison of the quench cracking resistance between Udimet 720LI and Rene'95 superalloys

		Solution temperature (°C)	Grain size ASTM	K_Q (MPa $\sqrt{m}$)	Failing temperature (°C)	Quench cracking mode
Fine grain structure	PM U720	1107	10.9	99–136	617–639	Intergranular/transgranular
	CW U720	1107	10.4	72–115	654–655	Intergranular/transgranular
	Rene'95	1100	12	17–24	936	Intergranular
Intermediate grain structure	PM U720	1107	7.0	38–49	868–914	Intergranular
		1168	7–8	31–47	934–954	Intergranular
	CW U720	1107	7.3	40–41	876–881	Intergranular
	Rene'95	1123–1181	7–8	7–16	894–1095	Intergranular

*Data from Ref. 11

imen before the jumping point and the precipitation of γ' after the jumping point.

Cooling Rate Effect. The effect of cooling rate on quench cracking behavior can also be interpreted by this softening and hardening competition. A lower cooling rate causes greater softening at high temperatures, at the beginning of the quenching process. Therefore, a lower cooling rate results in higher quench cracking resistance in fine and intermediate grain structure samples.

To conclude, if there are more grain boundaries, lower cooling rate, higher degree of softening, and more energy release at the beginning of the quenching, there is more possibility for the alloy to survive through the fracture mode transition temperature, and then higher quench cracking toughness is expected. Grain size effect and brittle/ductile fracture transition are also confirmed in the investigation of Rene'95 alloy. In that study, a transition temperature of 700 to 850 °C was suggested.[11]

Alloy Effect. Table 5 summarizes some comparative research results of both U720LI and Rene'95. The data of Rene'95 is from Ref 11. Either in fine grain structure or in intermediate grain structure, U720LI shows much higher cracking toughness than Rene'95. One of the reasons may be composition effect. Both alloys contain different amounts of γ' forming element. The U720LI alloy contains less Al and Ti and, thus, less γ' volume fraction. The ductility of U720LI is better than that of Rene'95 alloy. The effect of the composition of alloy on quench cracking behavior is still under investigation. Another reason may be the gage section size effect. The gage section size of the specimen used in U720LI research is different from that in Rene'95 research. In Rene'95 research, the specimen has a narrower gage width than that in U720LI test. So, it is reasonable to believe that the time allowed for a crack to develop in the narrow specimen is much shorter than in the wide specimen. In other words, the time allowed for thermal stress increase is shortened. Before the narrow specimen can reach the temperature for transition of fracture mode, it has already broken. That is why the narrow specimen exhibits a little lower cracking toughness under the same test conditions, according to our recent research. The effect of specimen size on quench cracking behavior is also under investigation. In general, in addition to having superior crack growth characteristics, Udimet 720LI has competitive high strength characteristics as compared with Rene'95. Consider-ing the quench capability, U720LI also shows higher quench cracking resistance.

5. Conclusions

- Quench cracking toughness K_Q is an effective tool to evaluate the quench cracking resistance of superalloys. Using the fracture mechanics approach, this study successfully demonstrated the quench cracking behavior of CW and PM superalloy Udimet 720LI. Quench cracking fracture is a completely brittle intergranular fracture mode at elevated temperature in fine grain structure or intermediate and coarse grain structure samples, which is different from that resulting from precracking, which shows transgranular fracture mode.
- Completely intergranular fracture in intermediate grain structure causes the lower quench cracking toughness at higher failing temperature. Fine grain structure shows higher quench cracking resistance and lower failing temperature, which contribute to the fracture mode transition from intergranular to transgranular during cooling. Grain size has a significant effect on quench cracking behavior of U720LI superalloy. What affects the transition temperature of fracture mode is under investigation.
- Cooling rate has a certain influence on the quench cracking resistance of U720LI materials. A higher cooling rate results in lower quench cracking toughness except for PMCG and CWIG alloys.
- PM U720LI with fine grain structure has higher quench cracking toughness than CW U720LI with the similar grain size. One of the reasons may be the inhomogeneous grain structure in CW U720LI.
- Udimet 720LI superalloy shows higher quench cracking resistance in comparison with Rene'95 superalloys.

References

1. Keh-Minn Chang: *Acta Metall. Sinica,* 1996, vol. 9(6), pp. 467-71.
2. Dwaine L. Klastrom: *Adv. Mater. Processes,* 1996, Apr., pp. 40EE-40HH.
3. Hiroshi Hattori, Mitsuhiro Takekawa, David Furrer, and Robert Noel: in *Superalloy 1996,* R.D. Kissinger, D.J. Deye, D.L. Anton, *et al.*, eds., TMS-AIME, Warrendale, PA, 1996, pp. 705-11.
4. Keh-Minn Chang, M.F. Henry, and M.G. Benz: *JOM,* 1990, vol. 42(12), pp. 29-35.
5. Chester F. Jatczak and Richard W. Brown: U.S. Patent No. 4,032,369, June 1977.

6. R.D. Kissinger: in *Superalloy 1996*, R.D. Kissinger, D.J. Deye, D.L. Anton, *et al.*, eds., TMS-AIME Warrendale, PA, 1996, pp. 689-95.
7. David R. Malley: U.S. Patent No. 4,654,091, Mar. 31, 1987.
8. Swami Ganesh, William R. Butts, and Raymond D. Rife: U.S. Patent No. 526,9857, Mar. 31, 1992.
9. Ramanath I. Ramakrishman and Timothy E. Howson: *JOM*, 1992, vol. 44(6), pp. 29-32.
10. Ronald A. Wallis: *Advanced Materials & Processes*, 1995, Sept., pp. 42kk-42NN.
11. Keh-Minn Chang and Boqun Wu: *1st Int. Non-Ferrous Processing and Technology, Conf. Proc.*, T. Bains and D.S. Mackenzie, eds., ASM International, Materials Park, OH, 1997, pp. 477-81.
12. Kenneth A. Green, Joseph A. Lemsky, and Robert M. Gasior: in *Superalloy 1996*, R.D. Kissinger, D.J. Deye, D.L. Anton, *et al.*, eds., TMS-AIME, Warrendale, PA, 1996, pp. 697-703.
13. K.R. Bain, M.L. Gambone, J.M. Hyzak, and M.C. Thomas: in *Superalloy 1988*, D.N. Duhl, G. Maurer, S. Antolovich, eds., TMS-AIME, Warrendale, PA, 1988, pp. 13-22.
14. D. Furrer and H. Fecht: *JOM*, 1999, Jan. pp. 33-36.
15. H. Tada, P. Paris, and G. Irvin: *The Stress Analysis of Cracks Handbook*, Del Research Corp., Hellertown, PA, 1973, pp. 2.10-2.12.
16. D. Furrer and H.-J. Fecht: *Scripta Mater.* 1999, vol. 40(11), pp. 1215-20.
17. Valerie L. Keefer: Master's Thesis, West Virginia University, Morgantown, WV, 1998.